IOP Publishing Journal of Physics B: Atomic, Molecular and Optical Physics
J. Phys. B: At. Mol. Opt. Phys. **49** (2016) 164005 (11pp) doi:10.1088/0953-4075/49/16/164005

Energy shift and state mixing of Rydberg atoms in ponderomotive optical traps

Xiao Wang[1] **and F Robicheaux**[1,2]

[1] Department of Physics and Astronomy, Purdue University, West Lafayette, IN 47907, USA
[2] Purdue Quantum Center, Purdue University, West Lafayette, IN 47907, USA

E-mail: robichf@purdue.edu

Received 1 April 2016
Accepted for publication 30 June 2016
Published 29 July 2016

Abstract

We present a degenerate perturbation analysis in the spin–orbit coupled basis for Rydberg atoms in an optical trap. The perturbation matrix is found to be nearly the same for two states with the same total angular momentum j, and orbital angular momentum number l differing by 1, The same perturbation matrices result in the same state-mixing and energy shift. We also study the dependence of state mixing and energy shift on the periodicity and symmetry of the ponderomotive potentials induced by different optical traps. State mixing in a one-dimensional lattice formed with two counterpropagating Gaussian beams is studied and yields a state-dependent trap depth. We also calculate the state-mixing in an optical trap formed by four parallel, separated and highly focused Gaussian beams.

Keywords: optical trapping, Rydberg atom, ponderomotive

(Some figures may appear in colour only in the online journal)

1. Introduction

Laser cooling and trapping of atoms have been important topics in the past couple decades. Optical trapping originates from the idea that neutral atoms can be polarized and have dipole energy in an oscillating electric field causing an energy shift that can be used to manipulate the atoms [1]. Optical trapping has some properties different from other atom traps, such as low trap-induced shifts, highly controllable trap depths. Typical optical trap induced shifts and trap depths are at the MHz level, and the effects caused by optical traps on the atomic internal states are extremely small [2]. These properties make optical trapping a very attractive system in different sub-fields. Optical trapping has been widely used in Bose–Einstein condensates [3], quantum computing [4], and other systems.

Innovative properties emerge when we use Rydberg atoms instead of ground state atoms in an optical trap due to the fact that the size of a Rydberg atom is comparable to the optical lattice period, which is the wavelength of laser beams. Ponderomotive optical traps are based on the fact that an electron oscillates with the same frequency of a highly oscillating electric field, and the time averaged kinetic energy acts as the trapping potential of the atom [5]. Recently, trapping Rydberg atoms based on the ponderomotive force has beeen studied in several works [5–7]. Most studies are related to a one-dimensional ponderomotive optical lattice formed by two counter-propagating Gaussian beams, since their interference gives a cosine shape beam intensity and trapping potential. Rydberg atoms in states with different principal quantum numbers n could feel different trapping depths, and the trapping depth in different nS states have been studied in [8].

Moreover, the angular distribution of the electron in a Rydberg atom also has a significant effect on the ponderomotive energy shift. Trapping properties of Rydberg atoms in high-l states in a one-dimensional lattice have been theoretically studied in [9]. Also the dependence of trap depth on the angular wavefunction has been experimentally studied in [7]. The dependence of ground-state atoms on magnetic quantum number m was studied in the late 1980s [10]. However, there has been no systematic theoretical analysis on the energy shift, trap depth and state mixing of Rydberg atoms with low-l in a ponderomotive potential including the effect of spin–orbit coupling (SOC). For atoms with small orbital angular momentum l, SOC can have significant effects on the angular distribution of electrons. These low-l states with SOC could have different trapping properties compared with nS states.

The state-dependent trap depths of Rydberg atoms provide a new technique that could be used in different systems.

The low trap-induced shifts and long coherence times of Rydberg atoms in a ponderomotive optical trap are advantages in different systems such as Bose–Einstein condensates of Rydberg atoms [11], high precision spectroscopy [12, 13], and quantum gate operations [14]. Also, we can change the parameters of the trap to minimize the difference of trap-induced shifts between ground and Rydberg states. This would give a high trapping efficiency when we excite atoms from ground states to Rydberg states [6].

In this paper, we present a degenerate perturbation analysis of a one-electron Rydberg atom in ponderomotive potentials including the effect of spin–orbit interactions. The method we use here is similar to that in [9]. We show that the energy shift and state mixing only depend on total angular momentum j, and there is almost no difference for two states with orbital angular momentum $l = j \pm 1/2$. In section 2.1, we present the origin of ponderomotive optical trapping, and the method we used for perturbation analysis. In section 2.2, we calculate the perturbation matrix in the degenerate spin–orbit coupled basis with given j. In sections 2.3 and 2.4, we study the state mixing under special symmetry and periodicity properties of the potential. In section 3, we give the numerical result of our analysis in two specific potentials: a one-dimensional lattice formed by two counterpropagating beams and an optical trap formed by four parallel and separated beams.

2. Theoretical analysis of the energy shift and state mixing

2.1. Introduction of ponderomotive force and ponderomotive energy

Optical trapping of a Rydberg atom originates from the ponderomotive force. A free electron in a highly oscillating electric field with amplitude E and angular frequency ω oscillates with the frequency of the field. The time averaged kinetic energy is given by

$$V = \frac{e^2E^2}{4m_e\omega^2}, \tag{1}$$

where $-e$ and m_e are the electron charge and mass, respectively. Thus, the time averaged kinetic energy of the electron acts as an effective potential energy for the atom.

Since a Rydberg electron has a large size distribution and spends most of its time far away from the atom nucleus, we can consider it as a quasi-free electron and calculate the spatial average of the ponderomotive potential. The atom nucleus has a much larger mass than the electron, so its ponderomotive energy is far smaller than the electron's and can be neglected here. Suppose the atom is in a space-dependent electric field, then the adiabatic ponderomotive shift can be calculated as [5]

$$V_{\rm ad}(\mathbf{R}) = \int \mathrm{d}^3\mathbf{r}\; V(\mathbf{r}+\mathbf{R})|\psi(\mathbf{r})|^2, \tag{2}$$

where $\mathbf{R}$ is the coordinate of nucleus, and $\mathbf{r}$ is the electron coordinate relative to the nucleus. $\psi(\mathbf{r})$ is the electron wavefunction in the Rydberg atom. $V(\mathbf{r}+\mathbf{R})$ is the space-dependent ponderomotive shift for a free electron, which is proportional to the square of electric field amplitude as in equation (1). The electric-field amplitude $E(\mathbf{r}+\mathbf{R})$ is time-independent as a result of laser-formed standing waves, which leads to a spatial potential $V(\mathbf{r}+\mathbf{R})$. Thus $V_{\rm ad}$ is the spatial average of the free electron ponderomotive energy weighted by the electron distribution in a given state $\psi(\mathbf{r})$. This space dependent potential $V_{\rm ad}(\mathbf{R})$ can be used as an optical atom trap.

This ponderomotive energy gives an extra potential in the Schrödinger equation and it can couple states together. However, since the energy, $V_{\rm ad}$, is usually not very large, we need to have degenerate or nearly degenerate states to have substantial mixing. The method we use is based on the degenerate perturbation theory, and we expand the perturbing potential in a degenerate or near degenerate basis. Then we diagonalize the perturbation matrix to study properties of energy shift and state mixing [9].

Suppose we have an atom in a set of degenerate or near degenerate states, e.g. ψ_1, ψ_2. Then the perturbation matrix can be calculated as

$$V_{\rm ad}(\mathbf{R}) = \begin{pmatrix} V_{\rm ad,11}(\mathbf{R}) & V_{\rm ad,12}(\mathbf{R}) \\ V_{\rm ad,21}(\mathbf{R}) & V_{\rm ad,22}(\mathbf{R}) \end{pmatrix}, \tag{3}$$

where

$$V_{{\rm ad},ij}(\mathbf{R}) = \int \mathrm{d}^3\mathbf{r}\; \psi_i^*(\mathbf{r})V(\mathbf{r}+\mathbf{R})\psi_j(\mathbf{r}). \tag{4}$$

Therefore, state ψ_1, ψ_2 can be coupled by the ponderomotive potential, and their degeneracy could be lifted due to the perturbation of the potential.

2.2. Perturbation matrices of atoms in different states

We write the Hamiltonian of a one-electron atom as

$$H = H_0 + H_{\rm SOC} + V, \tag{5}$$

where H_0 is the unperturbed Hamiltonian of the atom, $H_{\rm SOC}$ is the SOC correction, and V is the ponderomotive potential. The free electron ponderomotive shift can be obtained at the MHz level [8], which mainly depends on the power, focal diameter and wavelength of the laser beams used in experiments. For the $n = 50$ state of Rb, the spin–orbit splitting is zero for an s state, 818 MHz for a p state, 92.7 MHz for a d state, and 1.27 MHz for an f state [12, 13]. For Rb 50 S, P, or D Rydberg states, the ponderomotive shifts are approximately 10 MHz as described in section 3.1, which is much smaller than the corresponding spin–orbit splitting. In this case, we should consider the ponderomotive potential as a perturbation in the spin–orbit coupled basis. If the spin–orbit splitting is much smaller than the ponderomotive caused coupling between different l's or j's, we should consider the ponderomotive perturbation in the basis of pure orbital states.

We start with the atom in an $S_{1/2}$ state; this state is degenerate for $m_j = \pm 1/2$. The angular wavefunctions for these states are

$$\left| l=0, s=\frac{1}{2}, j=\frac{1}{2}, m_j=+\frac{1}{2} \right\rangle = |l=0, m_l=0\rangle \left| s=\frac{1}{2}, \uparrow \right\rangle, \tag{6}$$

$$\left| l=0, s=\frac{1}{2}, j=\frac{1}{2}, m_j=-\frac{1}{2}\right\rangle = |l=0, m_l=0\rangle \left| s=\frac{1}{2}, \downarrow\right\rangle. \quad (7)$$

Here $|\uparrow\rangle$ and $|\downarrow\rangle$ denote the electron in the spin-up and spin-down states, respectively. We use the method in section 2.1 to calculate the perturbation matrix. These matrix elements can be calculated as

$$V_{m_j,m_j'}(\mathbf{R}) = \langle n, l, j, m_j|V(\mathbf{R})|n, l, j, m_j'\rangle, \quad (8)$$

$$\begin{aligned} V_{\pm\frac{1}{2},\pm\frac{1}{2}}(\mathbf{R}) &= \left\langle m_j=\pm\frac{1}{2}\right| V(\mathbf{R}) \left|m_j'=\pm\frac{1}{2}\right\rangle, \\ &= \int \mathrm{d}^3\mathbf{r}\; V(\mathbf{r}+\mathbf{R})|\psi_{n00}(\mathbf{r})|^2 \cdot \langle\uparrow|\uparrow\rangle \text{ or } \langle\downarrow|\downarrow\rangle, \\ &= \int r^2\mathrm{d}r\; R^2(r) \int \mathrm{d}\Omega\; [Y_{00}^*(\theta,\varphi)Y_{00}(\theta,\varphi)]V(\mathbf{r}'), \quad (9) \end{aligned}$$

$$\begin{aligned} V_{\pm\frac{1}{2},\mp\frac{1}{2}}(\mathbf{R}) &= \left\langle m_j=\pm\frac{1}{2}\right| V(\mathbf{R}) \left|m_j'=\mp\frac{1}{2}\right\rangle, \\ &= \int \mathrm{d}^3\mathbf{r}\; V(\mathbf{r}+\mathbf{R})|\psi_{n00}(\mathbf{r})|^2 \cdot \langle\uparrow|\downarrow\rangle \text{ or } \langle\downarrow|\uparrow\rangle, \\ &= 0. \quad (10) \end{aligned}$$

Here $R(r)$ is the radial wavefunction of the Rydberg electron, and the $Y_{lm}(\theta,\varphi)$ are spherical harmonics. Note these matrix elements depend on the position of the nucleus, thus the perturbation matrix V is also position-dependent. That means the perturbation matrix has different eigenvalues when the atom is located at different positions in the potential. In equations (9) and (10), the ponderomotive potential shifts depend on the shape of the electric field in $V(\mathbf{R})$ from equation (1), on the radial wavefunction $R(r)$, and on the angular distribution of the electron. Rydberg states with the same n and small difference in l have similar radial distributions (e.g. nS, nP, and nD) on the distance scale over which $V(\mathbf{R})$ varies. The radius of their maximum radial distribution are approximately $2(n-\mu_{jl})^2$. The quantum defect μ_{jl} is small compared with the principal quantum number n of Rydberg states, and has a small relative effect on the radial wavefunction.

As a result, the angular part of the integrand of a matrix element $V_{m_j,m_j'}$ will be an important factor in the determination of the coupling between different states. If two matrix elements have the same radial wavefunction and angular integrand, they will have the same integral, which means the same perturbation matrix element. Also, if an angular integrand vanishes, its corresponding element also vanishes. Therefore, it is beneficial to investigate the properties of the angular integrand for different Rydberg states.

For convenience, we can write the angular part of the integrand from the wavefunctions as the matrix element of a new matrix, the angular matrix $\tilde{\rho}$. Extract the angular integrands from the wavefunctions in equations (9) and (10), the angular matrix elements $\tilde{\rho}_{m_j,m_j'}$ of $S_{1/2}$ state can be written as

$$\tilde{\rho}_{\pm\frac{1}{2},\pm\frac{1}{2}} = Y_{00}^*Y_{00}, \quad (11)$$

$$\tilde{\rho}_{\frac{1}{2},-\frac{1}{2}} = \tilde{\rho}_{-\frac{1}{2},\frac{1}{2}}^* = 0, \quad (12)$$

which can be written in the more compact form

$$\tilde{\rho} = \begin{pmatrix} Y_{00}^*Y_{00} & 0 \\ 0 & Y_{00}^*Y_{00} \end{pmatrix}. \quad (13)$$

We call this matrix the angular matrix of a one-electron system in Rydberg $S_{1/2}$ state.

Similar to the case for an $S_{1/2}$ state, if we consider the atom in a Rydberg $P_{1/2}$ state, we can use Clebsch–Gordan cofficients to convert the spin–orbit coupled basis into an orbital basis (angular part), which is

$$\left| l=1, s=\frac{1}{2}, j=\frac{1}{2}, m_j=+\frac{1}{2}\right\rangle = -\sqrt{\frac{1}{3}}\, Y_{10}\,|\uparrow\rangle + \sqrt{\frac{2}{3}}\, Y_{11}\,|\downarrow\rangle, \quad (14)$$

$$\left| l=1, s=\frac{1}{2}, j=\frac{1}{2}, m_j=-\frac{1}{2}\right\rangle = \sqrt{\frac{1}{3}}\, Y_{10}\,|\downarrow\rangle - \sqrt{\frac{2}{3}}\, Y_{1,-1}\,|\uparrow\rangle. \quad (15)$$

Matrix elements of the angular matrix of a $P_{1/2}$ state can be written as

$$\tilde{\rho}_{\pm\frac{1}{2},\pm\frac{1}{2}} = \frac{1}{3}Y_{10}^*Y_{10} + \frac{2}{3}Y_{11}^*Y_{11} = Y_{00}^*Y_{00}, \quad (16)$$

$$\tilde{\rho}_{\frac{1}{2},-\frac{1}{2}} = \tilde{\rho}_{-\frac{1}{2},\frac{1}{2}}^* = \frac{\sqrt{2}}{3}(Y_{11}^*Y_{10} + Y_{10}^*Y_{1,-1}) = 0, \quad (17)$$

which means all matrix elements of the angular matrix of $P_{1/2}$ state are exactly the same as for the $S_{1/2}$ state.

If we have the atom in a Rydberg $P_{1/2}$ state, no matter what shape the ponderomotive potential is, the two states $|m_j=\pm1/2\rangle$ are never mixed just as for the $S_{1/2}$ case. Each of them is an eigenstate of this system. They also have the same energy shift, which means the ponderomotive potential cannot split the $P_{1/2}$ state.

Similarly, we find that the angular matrix of the $P_{3/2}$, and $D_{3/2}$ states are the same:

$$\tilde{\rho} = \begin{pmatrix} Y_{11}^*Y_{11} & \sqrt{\frac{2}{3}}Y_{11}^*Y_{10} & \sqrt{\frac{1}{3}}Y_{11}^*Y_{1,-1} & 0 \\ \sqrt{\frac{2}{3}}Y_{11}Y_{10}^* & \frac{1}{3}Y_{11}^*Y_{11}+\frac{2}{3}Y_{10}^*Y_{10} & 0 & \sqrt{\frac{1}{3}}Y_{11}^*Y_{1,-1} \\ \sqrt{\frac{1}{3}}Y_{11}Y_{1,-1}^* & 0 & \frac{1}{3}Y_{11}^*Y_{11}+\frac{2}{3}Y_{10}^*Y_{10} & -\sqrt{\frac{2}{3}}Y_{11}^*Y_{10} \\ 0 & \sqrt{\frac{1}{3}}Y_{11}Y_{1,-1}^* & -\sqrt{\frac{2}{3}}Y_{11}Y_{10}^* & Y_{11}^*Y_{11} \end{pmatrix}. \quad (18)$$

Since equation (18) is an Hermitian matrix, we can use the fact that $Y_{lm}^* = (-1)^m Y_{l,-m}$, and the product of two spherical harmonics can be expanded as a linear combination of spherical harmonics. Then we can re-write the matrix

equation (18) as

$$\tilde{\rho} = \begin{pmatrix} \frac{5Y^*_{0,0}-\sqrt{5}Y^*_{2,0}}{10\sqrt{\pi}} & \frac{Y^*_{2,-1}}{\sqrt{10\pi}} & -\frac{Y^*_{2,-2}}{\sqrt{10\pi}} & 0 \\ -\frac{Y^*_{2,1}}{\sqrt{10\pi}} & \frac{5Y^*_{0,0}+\sqrt{5}Y^*_{2,0}}{10\sqrt{\pi}} & 0 & -\frac{Y^*_{2,-2}}{\sqrt{10\pi}} \\ -\frac{Y^*_{2,2}}{\sqrt{10\pi}} & 0 & \frac{5Y^*_{0,0}+\sqrt{5}Y^*_{2,0}}{10\sqrt{\pi}} & -\frac{Y^*_{2,-1}}{\sqrt{10\pi}} \\ 0 & -\frac{Y^*_{2,2}}{\sqrt{10\pi}} & \frac{Y^*_{2,1}}{\sqrt{10\pi}} & \frac{5Y^*_{0,0}-\sqrt{5}Y^*_{2,0}}{10\sqrt{\pi}} \end{pmatrix}. \tag{19}$$

With our definition of the angular matrix element $\tilde{\rho}_{ij}$, we may now calculate the perturbation matrix element in equation (4) in another way:

$$\begin{aligned} V_{ij}(\mathbf{R}) &= \langle\psi_i|V(\mathbf{R})|\psi_j\rangle \\ &= \int r^2 \mathrm{d}r\ R^2(r) \int \mathrm{d}\Omega\ \tilde{\rho}_{ij}(\theta,\varphi) V(\mathbf{R}+\mathbf{r}). \end{aligned} \tag{20}$$

We first do the radial part integral with the free electron ponderomotive potential $V(\mathbf{R}+\mathbf{r})$ and the radial wavefunction $R(r)$. We have

$$V_{ij}(\mathbf{R}) = \int \mathrm{d}\Omega\ \tilde{\rho}_{ij}(\theta,\varphi)\widehat{V}(\mathbf{R},\theta,\varphi), \tag{21}$$

where

$$\widehat{V}(\mathbf{R},\theta,\varphi) = \int r^2 \mathrm{d}r\ R^2(r) V(\mathbf{R}+\mathbf{r}). \tag{22}$$

Then we can expand $\tilde{\rho}_{ij}$ and $\widehat{V}$ in the spherical harmonic basis and its complex conjugate basis. We have

$$\widehat{V}(\mathbf{R},\theta,\varphi) = \sum_{lm} a_{lm}(\mathbf{R}) Y_{lm}(\theta,\varphi), \tag{23}$$

$$\tilde{\rho}_{ij}(\theta,\varphi) = \sum_{l'm'} b_{l'm'} Y^*_{l'm'}(\theta,\varphi). \tag{24}$$

Thus equation (21) can be simplified as

$$\begin{aligned} V_{ij}(\mathbf{R}) &= \int \mathrm{d}\Omega \sum_{lm}\sum_{l'm'} a_{lm}(\mathbf{R}) b_{l'm'} Y_{lm}(\theta,\varphi) Y^*_{l'm'}(\theta,\varphi), \quad (25) \\ &= \sum_{lm} a_{lm}(\mathbf{R}) \cdot b_{lm}. \end{aligned} \tag{26}$$

The last step is based on the orthonormality of the spherical harmonics. In equation (22), $\widehat{V}$ is the radial averaged free electron ponderomotive potential using the radial wavefunction. Thus $\widehat{V}$ is an angular function and it is nearly independent of quantum number l, m, or m_j. We can find the expression of a_{lm} in equation (23) using Fourier analysis. We have

$$\begin{aligned} a_{lm}(\mathbf{R}) &= \int \mathrm{d}\Omega\ \widehat{V}(\mathbf{R},\theta,\varphi) Y^*_{lm}(\theta,\varphi), \quad (27) \\ &= \int \mathrm{d}\Omega\ [Y_{lm}(\theta,\varphi)^*] \int r^2 \mathrm{d}r\ R^2(r) V(\mathbf{R}+\mathbf{r}). \end{aligned} \tag{28}$$

We name a_{lm} the multipole expansion value of a free electron ponderomotive potential $V(\mathbf{R})$ on the spherical haromonics Y_{lm} in the given radial wavefunction $R(r)$.

For a given potential, we can study its expansion values on different spherical harmonics to study the energy shift and state mixing for an electron in states with different l, m, or m_j. Usually the monopole term a_{00} is several times larger than the other higher order terms because spherical harmonics Y_{00} is always positive in θ and φ, thus there tends to be little cancelation in the integral for the matrix elements. Conversely, higher order spherical harmonics change sign in the integral region, and spherical harmonics with higher l, m flip sign more frequently than those with smaller l, m. Since positive and negative values are somewhat canceled, the higher order expansion values are usually smaller than the lower order expansion values. Because a_{00} only exists in the diagonal terms with $m_j = m'_j$, the diagonal elements are usually several times larger than the off-diagonal elements. We will study the properties of a_{lm} in potentials with symmetric properties in section 2.3.

For an electron in a spin–orbit coupled basis with given j and $l = j - 1/2$, the general expression for the element in the angular matrix, after tracing over the spin, can be written as

$$\begin{aligned} \tilde{\rho}^{(j)}_{m_j,m'_j} = {} & C_1 C'_1\ Y^*_{j-1/2,m_j-1/2} Y_{j-1/2,m'_j-1/2} \\ & + C_2 C'_2\ Y^*_{j-1/2,m_j+1/2} Y_{j-1/2,m'_j+1/2}. \end{aligned} \tag{29}$$

The element for j, $l = j + 1/2$ can be written as

$$\begin{aligned} \tilde{\rho}^{(j)}_{m_j,m'_j} = {} & C_3 C'_3\ Y^*_{j+1/2,m_j-1/2} Y_{j+1/2,m'_j-1/2} \\ & + C_4 C'_4\ Y^*_{j+1/2,m_j+1/2} Y_{j+1/2,m'_j+1/2}. \end{aligned} \tag{30}$$

These C_i, C'_i symbols are Clebash–Gordan coefficients. We can expand the product of two spherical harmonics into a linear combination of spherical harmonics, and simplify equations (29) and (30). They generate the same expansion result (see appendix for the derivation):

$$\tilde{\rho}^{(j)}_{m_j,m'_j} = \sum_{L=|m_j-m'_j|}^{2j-1} b(m_j, m'_j, L) \times Y^*_{L,m_j-m'_j}, \tag{31}$$

where

$$\begin{aligned} b(m_j, m'_j, L) = {} & (-1)^{m_j+1/2} \sqrt{\frac{2L+1}{4\pi}} \\ & \times \sqrt{(2j+1+L)(2j-L)} \begin{pmatrix} j-\frac{1}{2} & j-\frac{1}{2} & L \\ 0 & 0 & 0 \end{pmatrix} \\ & \times \begin{pmatrix} j & j & L \\ -m_j & m'_j & m_j - m'_j \end{pmatrix}. \end{aligned} \tag{32}$$

The brackets in equation (32) are Wigner 3j-symbol. We name this $b(m_j, m'_j, L)$ the expansion coefficient of an angular matrix element on spherical harmonics $Y^*_{L,m_j-m'_j}$. Note that all of the anti-diagonal matrix elements with $m_j + m'_j = 0$ vanish because of the parity in spherical haromonics. Also note that, according to equation (32), if $m_j = m'_j$ and $L = 0$, the coefficient multiplying the Y_{00} in the diagonal elements are all $1/\sqrt{4\pi}$. We will use this result for state mixing analysis in section 2.4. In equation (31), the summation index L is in the range $|m_j - m'_j| \leqslant L \leqslant 2j - 1$ and L must be an even integer for the expansion coefficient to be non-zero. That means only Y_{00}, Y_{2m}, Y_{4m}, etc terms exist in the angular matrices, and only monopole, quadrupole, hexadecapole, etc expansion values of the potential have an effect on the ponderomotive shift.

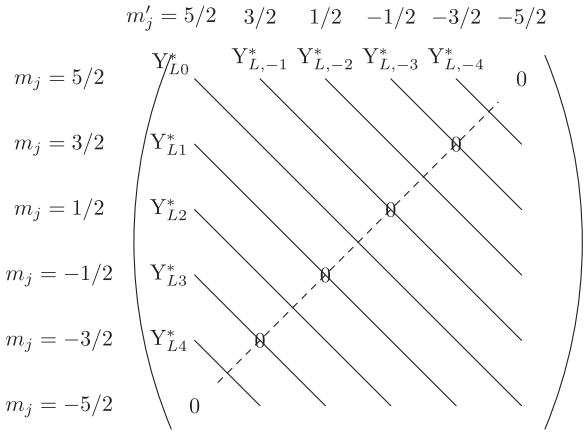

Figure 1. Angular matrix of $D_{5/2}$ state.

For example, we can use this analysis for the $D_{5/2}$ state to study the properties of its angular matrix. This is a 6×6 matrix, and we obtain the result in figure 1, where only diagonal elements contain summation of Y_{L0} terms. The first two off-diagonal lines have $Y_{L,\pm1}$ terms, while the second two off-diagonal lines have $Y_{L,\pm2}$ terms, etc. The dashed line in the matrix contains anti-diagonal elements, which are always zero. We will use this figure for symmetry analysis in section 2.3.

Angular matrices always have the same form for the two spin–orbit coupled states with the same j, and l differing by 1. In this case, if the energy shift induced by the ponderomotive potential is much smaller than that caused by the SOC, the total angular momentum number j determines the eigenvalues and eigenstates of the electron in a ponderomotive potential.

If we consider the atomic Hamiltonian without the SOC term, or if the spin–orbit splitting is much smaller than ponderomotive shift, the cross terms between different j's or l's will be important for obtaining the correct states and energies. If these cross terms are comparable to or larger than the spin–orbit splitting, states between different j's or l's have significant mixing. This usually happens for Rydberg states with $l \geqslant 3$. For example, the natural energy spliting between 50 $F_{5/2}$ and 50 $F_{7/2}$ states is 1.27 MHz [13], which is smaller than the cross terms between them (about 5–10 MHz) caused by two Gaussian beams with power 1 W as described in section 3.1. For electrons in these states, we need to calculate the perturbation matrix in a larger basis including $j = l \pm 1/2$ and other near degenerate states. This is equivalent to a pure orbital basis since electron spin has no explicit effect on ponderomotive potential. Properties of high-l atoms in ponderomotive potential have been studied in [9].

2.3. Symmetry analysis of the potential shape

We study those special potentials with rotational symmetry properties, and the effect of periodicity on the ponderomotive energy shift. Consider a potential with periodicity in φ, $V(r, \theta, \varphi) = V(r, \theta, \varphi + 2\pi/s)$, s is a positive integer, and $s \geqslant 2$. We use the conversion relation that $Y^*_{lm} = (-1)^m Y_{l,-m}$.

Then we calculate the integral in equation (27):

$$\begin{aligned}
&\int_0^{2\pi} \mathrm{d}\varphi\ V(\theta, \varphi) Y_{lm}(\theta, \phi), \\
=&\int_0^{2\pi} \mathrm{d}\varphi\ V(\theta, \varphi) f(\theta) \mathrm{e}^{\mathrm{i}m\varphi}, \\
=&\int_0^{2\pi/s} \mathrm{d}\varphi\ V(\theta, \varphi) f(\theta) [\mathrm{e}^{\mathrm{i}m\varphi} + \mathrm{e}^{\mathrm{i}m(\varphi + 2\pi\frac{1}{s})} \\
&+ \mathrm{e}^{\mathrm{i}m(\varphi + 2\pi\frac{2}{s})} + \ldots + \mathrm{e}^{\mathrm{i}m(\varphi + 2\pi\frac{s-1}{s})}], \\
=&\begin{cases}
\displaystyle\int_0^{2\pi/s} \mathrm{d}\varphi\ V(\theta, \varphi) f(\theta) \mathrm{e}^{\mathrm{i}m\varphi} \frac{1 - \exp(2\pi m\mathrm{i})}{1 - \exp(2\pi m\mathrm{i}/s)} = 0 \\
\quad \text{when } \exp(2\pi m\mathrm{i}/s) \neq 1, \\
\displaystyle\int_0^{2\pi/s} \mathrm{d}\varphi\ V(\theta, \varphi) f(\theta) \mathrm{e}^{\mathrm{i}m\varphi} \cdot s \\
\quad \text{when } \exp(2\pi m\mathrm{i}/s) = 1.
\end{cases}
\end{aligned} \tag{33}$$

When the common ratio $\exp(2\pi m\mathrm{i}/s)$ is not 1 in the geometric summation in equation (33), m is not a multiple of s, and the integral vanishes. This gives the result that the expansion value a_{lm} in equation (27) is zero. Based on the fact that $Y^*_{lm} = (-1)^m Y_{l,-m}$, both values $a_{l,\pm m}$ are zero. Conversely, for those m's which are multiples of s, the expansion values on these spherical harmonics do not vanish (zero is a multiple of any integer s).

For example, if a potential has φ-periodicity that $V(\varphi) = V(\varphi + \pi/2)$, we have $s = 4$. Multipole expansions of the potential with $M = 1, 2, 3, 5, 6, 7, \ldots$ vanish, while $M = 0, 4, 8, \ldots$ terms are non-zero. Suppose we have an atom in the $P_{3/2}$ or $D_{3/2}$ state. These two states have 4×4 angular matrices which can be found in equation (19), and the matrix elements consist of Y_{LM} with $|M| \leqslant 2$. Based on our analysis here, all of these off-diagonal matrix elements vanish for these two states, and only the diagonal elements are non-zero. As a result, $P_{3/2}$ and $D_{3/2}$ states would not mix in this periodic potential at this symmetric position.

Furthermore, suppose we have an atom in the $D_{5/2}$ state with the same periodic potential. In the angular matrix, only diagonal elements and $Y_{L,\pm4}$ elements are non-zero, and all other elements vanish. Refer to figure 1, only the elements in the diagonal line and $Y_{L,\pm4}$ lines have non-zero values. We will analyze state mixing in this kind of potential in section 2.4. Numerical results can be found in section 3.3.

There is an intersting limit when $s \to \infty$, and it means that this potential is cylindrically symmetric and φ-independent. In this case, only the $m = 0$ terms do not vanish. This means, in the angular matrix, only the diagonal terms are non-zero, and the spin–orbit coupled or orbital eigenstates are never mixed in this potential. We can also get this result directly from the fact that cylindrically symmetric potential conserves the magnetic quantum number m. In this kind of potential, we may get the ponderomotive energy shifts directly from calculating the expectation value of the potential in the unperturbed states [7].

Similarly, we study potentials satisfying symmetric properties $V(\theta) = V(\pi - \theta)$, which corresponds to potentials having a mirror symmetry with respect to the x–y plane.

We can calculate the integral (let $\theta' = \pi - \theta$)

$$\begin{aligned}&\int_0^{\pi} \mathrm{d}\theta\ \sin(\theta) V(\theta) P_l^m(\cos\theta),\\ &= \int_{\pi}^{0} -\mathrm{d}\theta'\ \sin(\theta') V(\theta') P_l^m(-\cos\theta'),\\ &= \int_0^{\pi} \mathrm{d}\theta'\ \sin(\theta') V(\theta') P_l^m(\cos\theta')(-1)^{l-m}. \end{aligned} \tag{34}$$

Here $P_l^m(\cos\theta)$ is the associated Legendre polynomial. Only even l are allowed in the matrix element expansion, so if m is an odd number, this integral vanishes. Therefore, only expansion values a_{LM} with both L, M even numbers are non-zero.

2.4. State mixing analysis based on symmetric potential

Some matrix elements vanish due to the symmetry properties of the potential and parity of the angular wavefunction. That leads to a simpler form of the perturbation matrix, and a simpler result for the state mixing. Generally, if a given potential does not have any special symmetry properties, most angular matrix elements are non-zero. In this case, expansion values a_{L1} exist, which would make state mixing between two adjacent spin–orbit coupled states with $\Delta m_j = 1$, and finally leads to complicated state mixing between almost all states.

We can review the following properties of matrix diagonalization in linear algebra. Suppose we have a diagonal matrix H with diagonal elements $h_{11} \sim h_{nn}$. The eigenstates of this matrix are just n unit vectors. Then we add a perturbation to this matrix by setting $h_{ij} = h_{ji}^* = p$, and let all the other off-diagonal elements remain zero. We can find that only the state i, j are mixed in the new eigenstates. Also, if the off-diagonal term is much smaller than the difference between two corresponding diagonal terms, which means $|p| \ll |h_{ii} - h_{jj}|$, the coupling between state i, j is small. Conversely, if $|p|$ is comparable to $|h_{ii} - h_{jj}|$, the coupling between state i, j gets much stronger.

In the perturbation matrix of $j = 3/2$ states in equation (19), all coefficients multiplying the Y_{00}^* terms in the diagonal elements are $1/\sqrt{4\pi}$. This is also a general result for the perturbation matrix in all states, and it can be derived from equation (32). Thus the a_{00} terms are the overall energy shifts for all states, and have no effect on state mixing. Refer to equation (19), the differences between diagonal terms originate in Y_{20}. Off-diagonal terms consist of $Y_{2,\pm1}$ and $Y_{2,\pm2}$. As we discussed in the last paragraph, if expansion values $a_{2,\pm1}$ or $a_{2,\pm2}$ are comparable to a_{20}, the coupling between states with $\Delta m_j = 1$, or 2 would be much stronger. Since a_{00} has no effect on the state mixing, the state mixing of a $j = 3/2$ state in a ponderomotive potential turns into analysis and comparison of the quadrupole expansions of the potential.

In our perturbation matrix, if a potential has symmetry properties and results in all a_{LM} with odd M vanishes, state mixing only exists between states with $\Delta m_j = 2$, and finally leads to state mixing among all states where Δm_j are even. Consider the 6×6 angular matrix for $D_{5/2}$ state in figure 1. If all a_{LM} with odd M vanish, the eigenstates would be states that mixed only within the two sets $m_j = 5/2, 1/2, -3/2$, and $m_j = 3/2, -1/2, -5/2$. Each set has 3 different methods of mixing. If we flip all signs of m_j in one mixing, we would get a corresponding mixed eigenstate in the other set with the same energy shift. As an example, both states $|\phi_1\rangle$, $|\phi_2\rangle$ in equations (35) and (36) are eigenstates in the ponderomotive potential, and they have the same energy shifts

$$|\phi_1\rangle = c_1 \left| m_j = \frac{5}{2} \right\rangle + c_2 \left| m_j = \frac{1}{2} \right\rangle + c_3 \left| m_j = -\frac{3}{2} \right\rangle, \tag{35}$$

$$\begin{aligned}|\phi_2\rangle = c_1^* &\left| m_j = -\frac{5}{2} \right\rangle\\ &+ c_2^* \left| m_j = -\frac{1}{2} \right\rangle + c_3^* \left| m_j = \frac{3}{2} \right\rangle. \end{aligned} \tag{36}$$

Since the angular momentum j_z of these two states have equal magnitudes but opposite signs, they would be split if we apply a small magnetic field B_z. We will study the properties of $|\phi_1\rangle$ instead of $|\phi_2\rangle$ or their linear combinations.

Furthermore, if we consider a potential with only a_{L0} and $a_{L,\pm4}$ expansion values, non-zero state mixing only exists between $\Delta m_j = 4$ such as the staes with $m_j = 5/2, -3/2$, and $m_j = 3/2, -5/2$. States $m_j = \pm 1/2$ are not mixed with any other states in this symmetric potential, and are, thus, eigenstates in the optical trap.

State mixing of an atom in a potential with these symmetry properties can be found in section 3.2.

3. Specific calculations for two traps

3.1. Counter-propagating beams as one-dimensional optical lattice

For an optical trap using two counter-propagating Gaussian beams in the experiment [6], the free electron ponderomotive potential can be written as

$$V(z) = \frac{e^2}{4m_e\omega^2} \times (E_0 \mathrm{e}^{\mathrm{i}kz} + E_0 \mathrm{e}^{-\mathrm{i}kz})^2, \tag{37}$$

$$= \frac{e^2 E_0^2}{m_e k^2 c^2} \times \cos^2(kz) \tag{38}$$

on the beam axis. The beam has a maximum intensity at $z = 0$, and a minimum at $z = \lambda/4$. We put an atom on the axis of the beam, and let the z-axis of the atom be the same with the beam axis. The atom would feel a cylindrically symmetric potential, which means it is φ-independent. Based on our analysis in section 2.3, spin–orbit coupled states will not mix in this potential.

We calculate the eigenvalues of a $D_{3/2}$ state when the atom locates on the different positions on the axis. Plot of eigenvalues versus z-position of the atom can be found in figure 2. Before perturbed by the ponderomotive potential, $D_{3/2}$ has 4 degenerate states which are $m_j = \pm 3/2, \pm 1/2$. After perturbation, we found two different eigenvalues when $z \neq \lambda/8$. The ponderomotive energy partially lifts the degenerace for $D_{3/2}$ states. States with the same absolute value of m_j are still degenerate. We also find that these two eigenvalues are the same at $z = \lambda/8$, which means a_{20} is zero

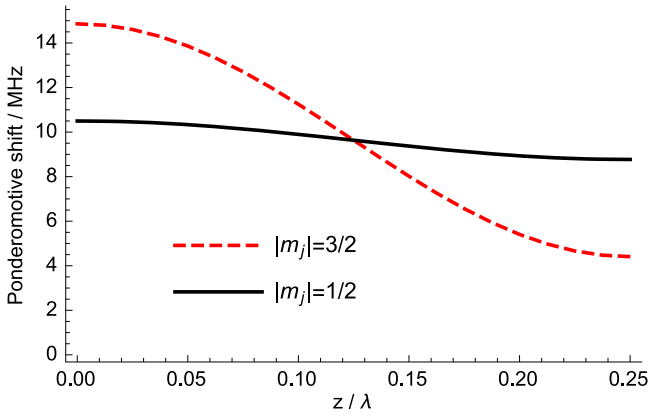

Figure 2. Eigenvalues of an atom in 50 $D_{3/2}$ state located on the beam axis in a ponderomotive optical lattice. Parameters used in our calculation are: $P = 1.0$ W, $\lambda = 1064$ nm, $\omega_0 = 6.5$ μm. These paremeters correspond to a free electron ponderomotive shift 19.3 MHz at $z = 0$.

at this point by comparing with the diagonal elements in equation (19). Therefore, the degeneracy of $D_{3/2}$ is not lifted at this point, and the state is still four-fold degenerate.

For the atom located at $z = z_0$, the potential can be simplified as

$$V(z, z_0) = V_0 \cos^2[k(z - z_0)], \tag{39}$$

$$= \frac{V_0}{2}\{1 + \cos[2k(z - z_0)]\}, \tag{40}$$

$$= \frac{V_0}{2}(1 + \cos 2kz_0 \cos 2kz + \sin 2kz_0 \sin 2kz). \tag{41}$$

In this expression, the ponderomotive potential consists of three parts. The first part $V_0/2$ is a constant shift, and its expansion in equation (28) only consists of monopole terms. It is the overall energy shift for all states. The third term $\sin 2kz$ has odd parity, and it vanishes in the integral with all Y_{LM} with even L. In the second term, $\cos 2kz_0$ is the atom position dependent coefficient, and it describes a cosine shape for the energy shift versus atom position z_0. Also, the spatial average of $V_2 = \cos 2kz$ in a specific eigenstate determines the trap depth in that state.

In figure 2, states with larger $|m_j|$ have larger trap depth. In those experiments with the atom in a DC electric field polarized perpendicular to the beam axis [7], atoms are in the Stark effect eigenstates with z-axis of the atom perpendicular to the beam axis. We can do similar analysis for the trap depth of atoms in these states with different $|m_j|$, and principal quantum number n. The analytic result is consistent with the experimental observation in [6].

3.2. Symmetric case in a system with four parallel Gaussian beams

A model for trapping atoms using four parallel Gaussian beams has been introduced in [15]. Each beam is centered at one corner of the square. Two diagonal beams have parallel

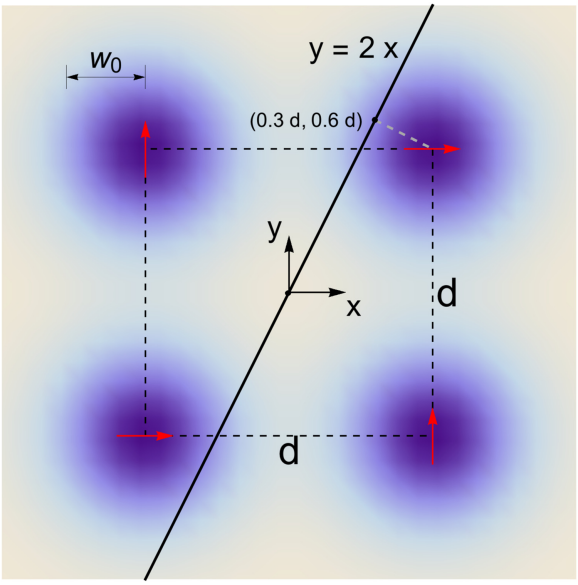

Figure 3. Setup of four parallel Gaussian beams system. Red arrows indicate the polarizations of beams. Parameters used in the calculation: $P = 5$ mW, $w_0 = 1.5$ μm, $d = 4$ μm, $\lambda = 780$ nm, where P is the power of one laser beam, w_0 is the waist of a beam, d is the distance between two adjacent beams, and λ is the wavelength. A free electron has a ponderomotive shift of 12.7 kHz at the center of the square, and 1.94 MHz at the center of one beam.

polarization, and two adjacent beams have perpendicular polarizations. The setup of this system can be found in figure 3 and figure 2 in [15]. This potential has good symmetries along the z-axis, $y = 0$ line, $y = x$ line, etc. It also has a mirror symmetry with respect to the $z = 0$ plane as described in section 2.3. We study the properties of an atom located at these symmetric positions in this section, and located at asymmetric positions in the next section.

Suppose the center of a cartesian frame is located at the center of the beam's square, and the z-axis is parallel with the beam axis. The free electron ponderomotive potential has the form

$$V(x, y, z) = \frac{e^2 E_0^2}{4 m_e \omega^2}\left[\frac{w_0}{w(z)}\right]^2 \left\{\left[u\left(x - \frac{d}{2}, y - \frac{d}{2}, z\right) + u\left(x + \frac{d}{2}, y + \frac{d}{2}, z\right)\right]^2 + \left[u\left(x - \frac{d}{2}, y + \frac{d}{2}, z\right) + u\left(x + \frac{d}{2}, y - \frac{d}{2}, z\right)\right]^2\right\}, \tag{42}$$

where

$$u(x, y, z) = \exp\left[-\frac{x^2 + y^2}{w^2(z)}\right]\exp[-\mathrm{i} \cdot \varphi(x, y, z)], \tag{43}$$

$$w(z) = w_0\sqrt{1 + \left(\frac{z}{z_R}\right)^2}, \tag{44}$$

$$\varphi(x, y, z) = kz + k\frac{x^2 + y^2}{2R(z)} - \eta(z), \tag{45}$$

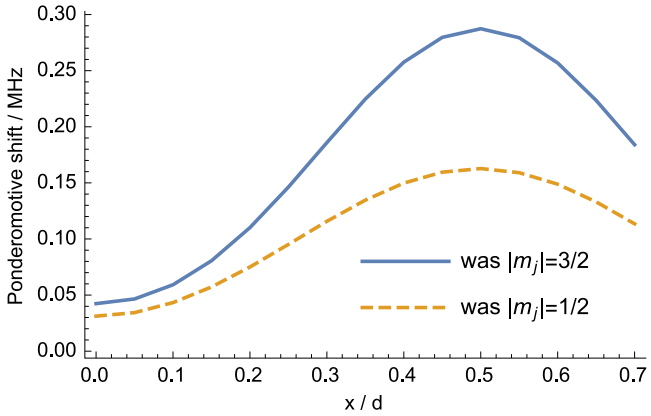

Figure 4. Energy shifts of an atom in 100 $D_{3/2}$ state located on the $y = 0$ line in the $z = 0$ plane. 'Was $|m_j| = 3/2$' means that when $x = 0$, the curve corresponds to the unmixed states $|m_j| = 3/2$.

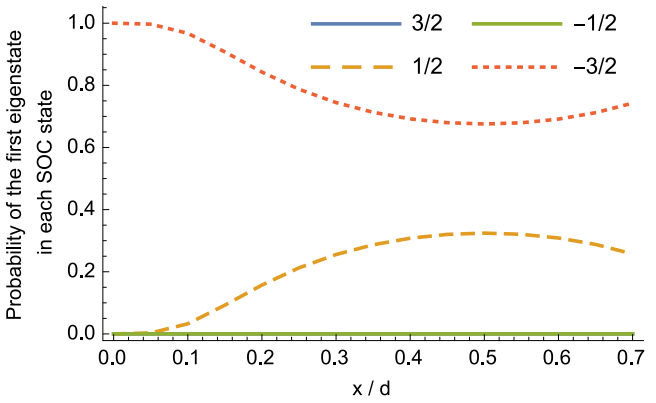

Figure 5. State mixing of an atom in 100 $D_{3/2}$ state located on the $y = 0$ line in the $z = 0$ plane. The vertical axis is the probability of the eigenstate in each SOC state m_j.

$$R(z) = z\left[1 + \left(\frac{z_R}{z}\right)^2\right], \tag{46}$$

$$\eta(z) = \arctan\left(\frac{z}{z_R}\right), \tag{47}$$

$$z_R = \frac{\pi w_0^2}{\lambda}. \tag{48}$$

The beam is highly focused so that the distance d is much larger than the beam waist w_0. This can reduce the effect of interference near $z = 0$ plane. As z increases, the waist size $w(z)$ increases, which increases the interference among these four beams.

We can investigate the properties of an atom in the 100 $D_{3/2}$ state and located on the $y = 0$ line in the $z = 0$ plane. The radius of this atom is approximately $2n^2a_0 \approx 1\mu$m, and it is comparable to d. Thus the energy shift and state mixing of this atom could have different properties when it is located at different positions in the potential. We can find from figure 3 that the potential has good symmetries when the atom is located on the $y = 0$ line in the $z = 0$ plane. When this atom is in the $z = 0$ plane, it feels a potential with $V(z) = V(-z)$. Based on our previous symmetry analysis in equation (34), all expansion values a_{LM} with odd M vanish. In addition, the atom feels the potential with a mirror symmetry $V(\varphi) = V(-\varphi)$. This kind of symmetric potential guarantees all of the perturbation matrix elements to be real, which leads to a real probability amplitude of the eigenstate in each spin–orbit coupled state. We plot the eigenvalues of the perturbation matrix in figure 4, and the probability of the corresponding eigenstate in each spin–orbit coupled state in figure 5.

The eigenvalue versus position curves have similar shapes with the free electron potential, which can be directly calculated from figure 3 and equation (42). They have the maximum energy shift at $x = 0.5\,d$ point. We also do the quadratic fit for this potential near the center $x = y = z = 0$, and the oscillating frequency of an Rb atom is of the order of 3–10 kHz in the x–y plane. The exact frequency depends on the wavefunction and the oscillating angle of the atom [15].

In figure 5, when the atom in a 100 $D_{3/2}$ state is located at the center $x = y = z = 0$ position, four m_j states are not mixed, which is because the potential has a $\pi/2$ angle rotational symmetry on φ at the center of the system. This figure shows the probability of the new eigenstates with $m_j = -3/2$ character at $x = 0$ in each SOC state. It gives the state coupling only between $m_j = -3/2$ and $m_j = 1/2$ states. Note that states $m_j = -1/2, 3/2$ have no contribution to this state mixing because expansion values $a_{l,\pm1}$ and $a_{l,\pm3}$ vanish due to the property of a mirror symmetric potential described in equation (34). State mixing only exists between $\Delta m_j = 2$. The state mixing gets stronger with the x-position of the atom, and reaches the maximum mixing at $x = 0.5\,d$ which is the closest position to the center of two adjacent Gaussian beams on this line.

Based on our analysis in equations (35) and (36), we can flip the sign of all m_j's in the first eigenstate, use the complex conjugate of their probability amplidutes as new amplitudes, and then we can get the second eigenstate for this system with the same energy (for convenience, we call the eigenstate in equation (5) the first eigenstate). There are also two other degenerate eigenstates with different energies from the first and second eigenstates. We can diagonalize a 4×4 perturbation matrix with a_{LM} vanishing for odd M, and get the analytic result for the other two eigenstates. If we write the first eigenstate as $c_1|1/2\rangle + c_2|-3/2\rangle$, the third eigenstate can be written as $c_1|3/2\rangle - c_2|-1/2\rangle$, and the fourth eigenstate can be written as $-c_2^*|1/2\rangle + c_1^*|-3/2\rangle$. Note here the first and the fourth eigenstates have their probabilities of $|1/2\rangle$ and $|-3/2\rangle$ exchanged, so does other two eigenstates.

Similarly, we can investigate the properties of an atom in 100 $D_{3/2}$ state and located on the $y = 2x$ line in the $z = 0$ plane. The potential still has z-symmetric properties, and only states with even Δm_j can mix in the eigenstates. Since the atom is no longer located on the $y = 0$ line, most of the perturbation matrix elements are no longer real numbers. The probability amplitudes of the eigenstates in the spin–orbit coupled states could be complex numbers. We plot eigenvalues in figure 6, and the probability of the eigenstates in each spin–orbit coupled state is shown in figure 7.

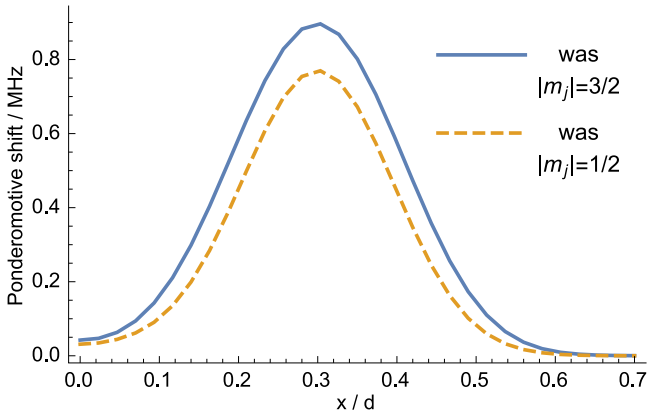

Figure 6. Energy shifts of an atom in 100 $D_{3/2}$ state located on the $y = 2x$ line in the $z = 0$ plane. 'Was $|m_j| = 3/2$' means that when $x = 0$, the curve corresponds to the unmixed states $|m_j| = 3/2$.

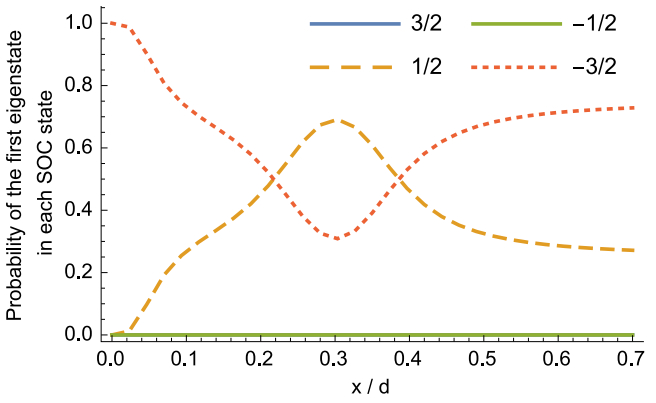

Figure 7. State mixing of an atom in 100 $D_{3/2}$ state located on the $y = 2x$ line in the $z = 0$ plane. The vertical axis is the probability of the eigenstates in each SOC state m_j.

We can find from figure 6 that the eigenvalues reach the maximum when the atom is located at $(x, y) = (0.3\,d, 0.6\,d)$, which is the closest position to the center of $(d/2, d/2)$ Gaussian beam on this line. The strongest state mixing of these two states appears at the same position in figure 7.

3.3. Asymmetric case in a system with four parallel Gaussian beams

As another example, we consider an atom in the state of 100 $D_{5/2}$, but let the atom locate on the line of $y = 2x$ in the $z = 5\ \mu$m plane. All other parameters of the optical trap remain the same with section 3.2.

Since the atom is no longer in the $z = 0$ plane, it does not have the mirror symmetry that exists for the $z = 0$ plane. Then the expansion values on Y_{LM} with odd M terms become non-zero on the line of $y = 2x$. Based on our analysis in section 2.4, the state coupling with $\Delta m_j = 1$ exists. As $z = 5\ \mu$m plane is close to the $z = 0$ plane, these odd M expansion values a_{LM} are small compared to the even M expansion values. As a result, the state mixing is mainly between $\Delta m_j = 2$ states, and only has small corrections for the other three states. Our calculated results of the eigenvalues versus the position of the atom can be found in figure 8, and three plots of the six eigenstates after mixing can be found in figure 9.

We find that wavefunctions of different eigenstates have substantial difference at different positions in this potential, though their energy shifts are similiar between each other.

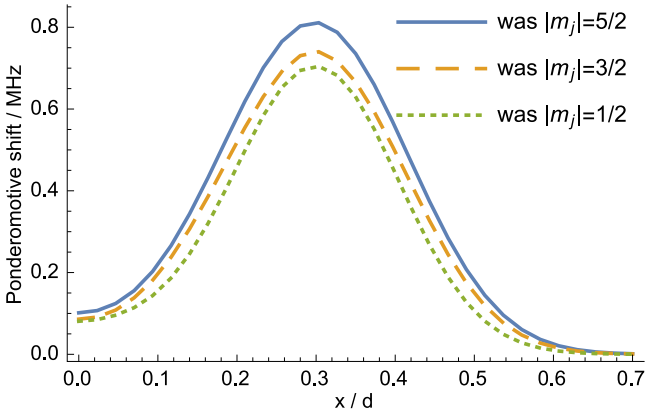

Figure 8. Energy shifts of an atom in 100 $D_{5/2}$ state located on the $y = 2x$ line in the $z = 5\ \mu$m plane. 'Was $|m_j| = 5/2$' means that when $x = 0$, the curve corresponds to the eigenstate mixed between $m_j = \pm 5/2$ and $\mp 3/2$, where $\pm 5/2$ is the main component of this state. 'Was $|m_j| = 3/2$' means the eigenstate mixed between $\pm 3/2$ and $\mp 5/2$, where $\pm 3/2$ is the main component. 'Was $|m_j| = 1/2$' means the eigenstate of $\pm 1/2$, and it was not mixed when $x = 0$.

4. Conclusions

In this paper, we investigated the effect of the ponderomotive force on a one-electron Rydberg atom. Using the wavefunction of a Rydberg electron, the spatial averaged ponderomotive energy of the Rydberg electron in an oscillating electric field acts as an effective potential energy of the Rydberg atom. This ponderomotive potential can couple degenerate or nearly degenerate states. Under the condition that the ponderomotive shift is much smaller than the SOC energy when $l \leqslant 3$, the effect of a ponderomotive potential can be analyzed using the degenerate perturbation theory in a spin–orbit coupled basis. We studied the energy shift and state mixing of a one-electron Rydberg atom with given orbital angular momentum l and total angular momentum j in different ponderomotive potentials.

First, we did multipole expansion of a ponderomotive potential. Then we studied matrix elements of a general spherical harmonics in a spin–orbit coupled basis to study the effect of spin–orbit coupled states' wavefunctions on the perturbation matrix. Our derivations showed that the eigenvalues and eigenstates mainly depend on j and n but hardly depend on l. As a result, the $|m_j = \pm 1/2\rangle$ states for $j = 1/2$ are never mixed in a ponderomotive potential.

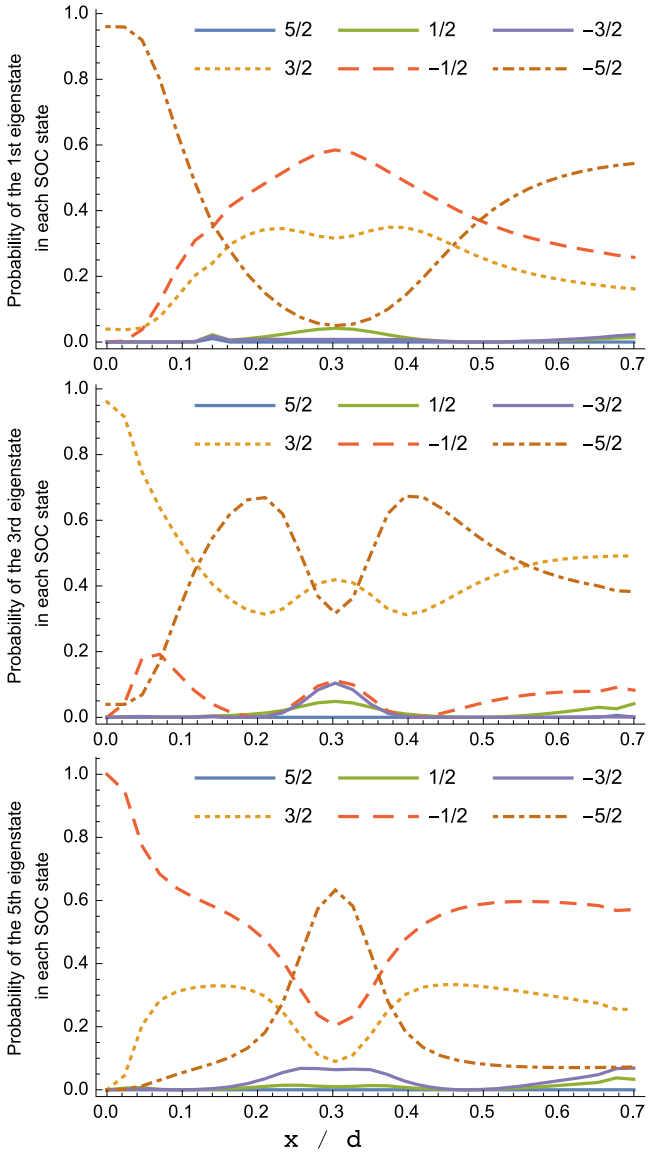

Figure 9. State mixing of an atom in 100 $D_{5/2}$ state located on the $y = 2x$ line in the $z = 5$ μm plane. The vertical axis is the probability of the eigenstates in each SOC state m_j. These graphs show the state mixing mainly among the states with $m_j = -\frac{5}{2}, -\frac{1}{2}, \frac{3}{2}$.

Some potentials have periodicity or symmetry properties. Under special symmetries, expansion values of some spherical harmonics in a given potential vanish. These zero matrix elements are usually on off-diagonal lines of the perturbation matrix, and lead to a simpler ponderomotive energy shift and state mixing. If the expansion value of a ponderomotive potential in Y_{LM} is zero, there is usually no state mixing between $\Delta m_j = M$ states. This gives a method to study the state mixing between two states by directly calculating the expansion value of the given potential in spherical harmonics. State mixing in this symmetric situation is still valid approximately if the atom is only slightly deviated from the symmetric or periodic position, because the expansion values of the potential in Y_{LM} remain very small even if they are not exactly zero.

We also calculated state mixing and energy shift in a one-dimensional optical lattice formed by two parallel Gaussian beams. Since this potential is cylindrically symmetric, there is no state mixing in this potential. Our result shows that energy shifts of different states are cosine functions versus the atom position on the beam axis. We also analyze the trap depth for states with different angular momentum in this potential, which mainly depends on the polarization direction, $|m|$ or $|m_j|$, and the principal quantum number of the state.

Acknowledgments

XW would like to thank Baochun Yang for helpful discussions. This material is based upon work supported by the US National Science Foundation under Grant No. 1404419-PHY.

Appendix. Proving the equivalence of two angular matrices for $(l = j - 1/2)_j$ and $(l = j + 1/2)_j$ states

Based on our definition of angular matrices in equation (13), each element is the angular part of the integrand of corresponding perturbation matrix element integral. In our derivation in equation (24), we expand the angular matrix element $\tilde{\rho}_{m_j,m_j'}$ on a basis of complex conjugate of spherical harmonics:

$$\tilde{\rho}_{m_j,m_j'}(\theta, \varphi) = \sum_{kq} b_{kq}(m_j, m_j')\, Y_{kq}^*(\theta, \phi). \tag{A.1}$$

Then we can calculate the matrix element of Y_{kq} in the spin–orbit coupled basis $\left| l = j \pm \frac{1}{2}, s = \frac{1}{2}, j, m_j \right\rangle$ to get the coefficient $b_{kq}(m_j, m_j')$, which is

$$b_{kq}(m_j, m_j') = \int \mathrm{d}\Omega\; Y_{kq}(\theta, \varphi)\tilde{\rho}_{m_j,m_j'}(\theta, \varphi), \tag{A.2}$$

$$= \left\langle l, s, j, m_j \middle| Y_{kq} \middle| l, s, j, m_j' \right\rangle. \tag{A.3}$$

Using the Wigner–Eckart theorem [16], we have

$$b_{kq}(m_j, m_j') = (-1)^{j-m_j} \begin{pmatrix} j & k & j \\ -m_j & q & m_j' \end{pmatrix} \times \langle l, s, j || Y^{(k)} || l, s, j \rangle, \tag{A.4}$$

$$= (-1)^{j-m_j} \begin{pmatrix} j & k & j \\ -m_j & q & m_j' \end{pmatrix} (-1)^{l+s+j+k}(2j+1) \times \begin{Bmatrix} l & j & s \\ j & l & k \end{Bmatrix} \langle l || Y^{(k)} || l \rangle, \tag{A.5}$$

$$= (-1)^{2j-m_j+l+s+k} \begin{pmatrix} j & k & j \\ -m_j & q & m_j' \end{pmatrix} (2j+1) \begin{Bmatrix} l & j & s \\ j & l & k \end{Bmatrix} \times (-1)^l \sqrt{\frac{(2l+1)^2(2k+1)}{4\pi}} \begin{pmatrix} l & k & l \\ 0 & 0 & 0 \end{pmatrix}, \tag{A.6}$$

$$= (-1)^{3/2-m_j+k}\begin{pmatrix} j & k & j \\ -m_j & q & m_j' \end{pmatrix}(2j+1)(2l+1)\begin{Bmatrix} l & j & \frac{1}{2} \\ j & l & k \end{Bmatrix} \times \sqrt{\frac{2k+1}{4\pi}}\begin{pmatrix} l & k & l \\ 0 & 0 & 0 \end{pmatrix}. \tag{A.7}$$

Here we used the fact that $s = 1/2$, $l = j \pm 1/2$. We must have some restrictions so that the matrix element is non-zero, which are

$$q = m_j - m_j', \tag{A.8}$$

$$|m_j - m_j'| \leqslant k \leqslant 2j, \tag{A.9}$$

$$k \text{ must be an even number}, \tag{A.10}$$

$$\Rightarrow |m_j - m_j'| \leqslant k \leqslant 2j - 1. \tag{A.11}$$

The explicitly l-dependent terms of equation (A.7) are as follows

$$c(l) = (2l+1)\begin{Bmatrix} l & j & \frac{1}{2} \\ j & l & k \end{Bmatrix}\begin{pmatrix} l & k & l \\ 0 & 0 & 0 \end{pmatrix}, \tag{A.12}$$

which can be shown to be the same for $l = j \pm 1/2$ [17]. The final form of equation (A.7) can be written as

$$b_{kq}(m_j, m_j') = (-1)^{m_j+1/2}\sqrt{\frac{2k+1}{4\pi}}\sqrt{(2j+k+1)(2j-k)} \times \begin{pmatrix} j-\frac{1}{2} & j-\frac{1}{2} & k \\ 0 & 0 & 0 \end{pmatrix}\begin{pmatrix} j & j & k \\ -m_j & m_j' & m_j - m_j' \end{pmatrix} \tag{A.13}$$

for $l = j \pm 1/2$, where $q = m_j - m_j'$. $b_{kq}(m_j, m_j')$ are non-zero only when k satisfies the restrictions in equations (A.10) and (A.11).

References

[1] Ashkin A 1997 Optical trapping and manipulation of neutral particles usinglasers *Proc. Natl Acad. Sci.* **94** 4853–60

[2] Grimm R, Weidemüller M and Ovchinnikov Y B 2000 Optical dipole traps for neutral atoms *Advances In Atomic, Molecular, and Optical Physics* vol 42 (New York: Academic), pp 95–170

[3] Stamper-Kurn D M, Andrews M R, Chikkatur A P, Inouye S, Miesner H-J, Stenger J and Ketterle W 1998 Optical confinement of a Bose–Einstein condensate *Phys. Rev. Lett.* **80** 2027–30

[4] Weitenberg C, Kuhr S, Mølmer K and Sherson J F 2011 Quantum computation architecture using optical tweezers *Phys. Rev.* A **84** 032322

[5] Dutta S K, Guest J R, Feldbaum D, Walz-Flannigan A and Raithel G 2000 Ponderomotive optical lattice for Rydberg atoms *Phys. Rev. Lett.* **85** 5551–4

[6] Anderson S E, Younge K C and Raithel G 2011 Trapping rydberg atoms in an optical lattice *Phys. Rev. Lett.* **107** 263001

[7] Anderson S E and Raithel G 2012 Dependence of Rydberg-atom optical lattices on the angular wave function *Phys. Rev. Lett.* **109** 023001

[8] Younge K C, Knuffman B, Anderson S E and Raithel G 2010 State-dependent energy shifts of Rydberg atoms in a ponderomotive optical lattice *Phys. Rev. Lett.* **104** 173001

[9] Younge K C, Anderson S E and Raithel G 2010 Adiabatic potentials for rydberg atoms in a ponderomotive optical lattice *New J. Phys.* **12** 023031

[10] Dalibard J and Cohen-Tannoudji C 1989 Laser cooling below the doppler limit by polarization gradients: simple theoretical models *J. Opt. Soc. Am.* B **6** 2023–45

[11] Viteau M, Bason M G, Radogostowicz J, Malossi N, Ciampini D, Morsch O and Arimondo E 2011 Rydberg excitations in Bose–Einstein condensates in quasi-one-dimensional potentials and optical lattices *Phys. Rev. Lett.* **107** 060402

[12] Li W, Mourachko I, Noel M W and Gallagher T F 2003 Millimeter-wave spectroscopy of cold rb Rydberg atoms in a magneto-optical trap: quantum defects of the *ns*, *np*, and *nd* series *Phys. Rev.* A **67** 052502

[13] Han J, Jamil Y, Norum D V L, Tanner P J and Gallagher T F 2006 Rb *nf* quantum defects from millimeter-wave spectroscopy of cold ^{85}Rb Rydberg atoms *Phys. Rev.* A **74** 054502

[14] Isenhower L, Urban E, Zhang X L, Gill A T, Henage T, Johnson T A, Walker T G and Saffman M 2010 Demonstration of a neutral atom controlled-not quantum gate *Phys. Rev. Lett.* **104** 010503

[15] Zhang S, Robicheaux F and Saffman M 2011 Magic-wavelength optical traps for Rydberg atoms *Phys. Rev.* A **84** 043408

[16] Edmonds A R 1996 *Angular Momentum in Quantum Mechanics* (Princeton, NJ: Princeton University Press) ch 5.4, 7.1

[17] Varshalovich D A, Moskalev A N and Khersonskii V K 1988 *Quantum Theory of Angular Momentum* (Singapore: World Scientific) ch 8.5.2, 9.12